Available online at www.sciencedirect.com
SCIENCE DIRECT®
International Journal of Multiphase Flow 31 (2005) 571–592
International Journal of Multiphase Flow
www.elsevier.com/locate/ijmulflow

Calculations of stratified wavy two-phase flow in pipes

Petter Andreas Berthelsen *, Tor Ytrehus

The Fluids Engineering Group, Department of Energy and Process Engineering, Norwegian University of Science and Technology, Kolbjørn Hejes vei 2, N-7491 Trondheim, Norway

Received 5 May 2004; received in revised form 30 January 2005

Abstract

Calculations of fully developed, stratified wavy gas–liquid pipe flow is presented. The wavy interface is represented by an equivalent interfacial roughness obtained from experimental data, which is made non-dimensional following the Charnock formulation. The two-dimensional, steady-state axial momentum equation is solved together with a two-layer turbulence model, which is modified to account for the roughness introduced at the interface. The governing equations are discretized using a finite difference method on a composite, overlapping grid with local grid refinement near the interface and the wall. The immersed interface method is used to make the numerical scheme well-defined across the interface, and a level set function is used to represent the interface. Numerical calculations are found to compare satisfactorily with experimental data.

Keywords: Stratified flow; Waves; Interfacial roughness; Multiphase flow; Immersed interface method; Level set function

1. Introduction

The stratified flow pattern is considered to be among the simple ones for gas–liquid flow; however, it is far from completely understood. The lack of details is mainly due to the wavy nature of

* Corresponding author. Present address: Centre for Ships and Ocean Structures, Norwegian University of Science and Technology, N-7046 Trondheim, Norway. Tel.: +47 73 55 11 05; fax: +47 73 59 55 28.
E-mail addresses: petter.a.berthelsen@ntnu.no (P.A. Berthelsen), tor.ytrehus@ntnu.no (T. Ytrehus).

0301-9322/$ - see front matter
doi:10.1016/j.ijmultiphaseflow.2005.02.001

the interface and the interaction between the deformed interface and the flow structure in both phases. Numerous experimental studies of local flow properties have been devoted to stratified wavy gas–liquid flow, but difficulty in making accurate measurements close to the interface limits our insight in this flow regime.

Most common models for industrial applications are based on greatly simplified representation of the flow structure. Mechanistic models are applied with common assumptions that both phases are treated as one-dimensional bulk flows. The shear stresses are calculated from empirical correlations based on the average velocity. Early approaches used modified correlations for single-phase flow, such as the well-known Blasius formula (e.g. Agrawal et al., 1973; Russel et al., 1974; Taitel and Dukler, 1976).

Later attempts have focused on finding better correlations for the friction terms where two-phase flow effects have been incorporated into the model. The interfacial shear stress has been mainly modelled by two different approaches for stratified wavy flow. In the most common approach, a global empirical correlation for the interfacial friction factor or the interfacial friction term is obtained from experimental data. Among others, the models proposed by Andreussi and Persen (1987), Andritsos and Hanratty (1987), and Biberg (1999) are based on this method. The other approach considers the analogy between the flow above a wavy interface and the flow above a rough surface where an empirical correlation for the interfacial roughness is proposed. Charnock (1955) linked the surface roughness to the frictional velocity through a non-dimensional parameter for waves in deep water. Rosant (1983) modified the Charnock relation for pipe flow. The Charnock relation may be used together with Colebrook's (1939) equation for flow in rough pipes.

There is a growing interest in exploring the possibilities in using computational fluid dynamics (CFD) to predict multiphase flow behaviour. Several attempts have been made to model and compute the details of wavy gas–liquid flow in rectangular channels, including those of Akai et al. (1980, 1981), Issa (1988), Liné et al. (1996), and Lorencez et al. (1997). For pipe flow, Shoham and Taitel (1984) discretized and solved the steady-state axial momentum equation in the liquid region using a bipolar coordinate system and a mixing-length turbulence model. The gas region was treated as a bulk flow, and an empirical correlation was used to couple the two phases through the interfacial shear stress. Issa (1988) extended his channel flow analysis to pipe flow using the bipolar coordinate system. He used a two-equation turbulence model with wall functions to calculate the flow field in both phases, but the results were restricted to smooth interfaces only.

Newton and Behnia (2001) extended their previous two-dimensional model of stratified smooth pipe flow (Newton and Behnia, 2000) to allow for interfacial waves. They applied a low Reynolds number k–ε turbulence model, which resolved the flow in the vicinity of the wall and the interface. A simple empirical shear stress distribution was imposed on the interface to modify their model for stratified wavy flow. Meknassi et al. (2000) introduced an interfacial roughness, which they included in the wall functions, to predict stratified wavy two-phase flow. Their study extended the work of Liné et al. (1996) to circular pipes, and the effect of secondary flow was included using an anisotropic turbulence model.

Recently, Berthelsen and Ytrehus (2004, 2005) developed a new two-dimensional numerical technique to calculate stratified smooth two- and three-phase pipe flow. The immersed interface method (Berthelsen, 2004a) was used to treat the interfacial boundary condition properly, where

the interfaces were represented by level set functions. This approach allows for using multiple and arbitrary shaped interfaces, regardless of the numerical grid structure. The primary purpose of the present work is to extend this technique to also include the effect of interfacial waves in gas–liquid flow. The wavy interface is treated as a rough surface. Turbulent stresses are modelled using a two-layer turbulence model. The two-layer turbulence model resolves the flow in the immediate vicinity of the wall and the interface, and it allows for direct predictions of the shear stress distribution along the boundaries.

2. Mathematical formulation

2.1. Momentum equation

In fully developed, incompressible pipe flow of stratified fluids, the time-averaged steady-state axial momentum equation for each phase can be written as

$$\frac{\partial}{\partial x}\left(\mu_e \frac{\partial u}{\partial x}\right) + \frac{\partial}{\partial y}\left(\mu_e \frac{\partial u}{\partial y}\right) - \frac{\mathrm{d}p}{\mathrm{d}z} - \rho g \sin\theta = 0, \tag{1}$$

where u is the axial velocity, ρ is the density, g is the gravitational acceleration, θ is the pipe inclination angle and $\mathrm{d}p/\mathrm{d}z$ is the pressure gradient in the axial direction. The effective viscosity, μ_e, is defined as the sum of molecular and turbulent viscosity denoted by μ and μ_t, respectively.

The interface is represented by the zero level of a smooth function ϕ (Osher and Sethian, 1988). This auxiliary function is defined as the signed distance to the interface,

$$\phi(x,y) = \pm d_\phi,$$

where the sign of ϕ indicates on which side of the interface the point (x,y) is located. The fluid properties can be defined directly from the level set function as (see Fig. 1)

$$\rho(\phi) = \begin{cases} \rho_L & \text{if } \phi < 0, \\ \rho_G & \text{if } \phi \geqslant 0, \end{cases} \quad \text{and} \quad \mu(\phi) = \begin{cases} \mu_L & \text{if } \phi < 0, \\ \mu_G & \text{if } \phi \geqslant 0, \end{cases}$$

assuming the interface to be infinitely thin. The subscripts L and G denote the liquid phase and gas phase, respectively.

Using the level set formulation, the interface does not need to be represented as a parameterized curve; its location is determined when ϕ vanishes. Another advantage with this method is that for

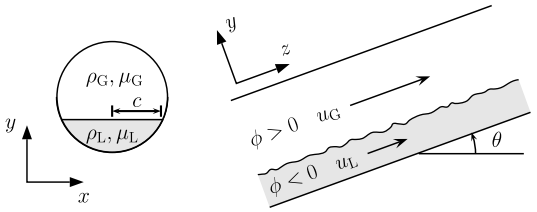

Fig. 1. Illustration of stratified wavy two-phase flow with definition of sign convention.

any given point (x, y) the exact distance to the interface is known. This becomes beneficial when evaluating the wall-damping functions in the turbulence model.

2.2. Turbulence modelling

A revised version of Chen and Patel's (1988) two-layer turbulence model is adopted to provide a closure relation for the turbulent viscosity μ_t. This two-layer approach is modified accordingly to Patel and Yoon (1995) and Durbin et al. (2001) to include the effect of interfacial waves or roughness. It consists of a standard two-equation k–ε model which is used only in the outer region away from surfaces, while the viscous-affected inner regions near physical boundaries are resolved with a simpler one-equation k–ℓ model.

The eddy viscosity relation is written as

$$\mu_t = C_\mu \rho \sqrt{k} \ell_\mu, \tag{2}$$

where C_μ is a dimensionless constant (see Table 1) and ℓ_μ is the turbulence length scale. The turbulent kinetic energy, k, is determined by the model equation

$$\frac{\partial}{\partial x}\left(\mu_k \frac{\partial k}{\partial x}\right) + \frac{\partial}{\partial y}\left(\mu_k \frac{\partial k}{\partial y}\right) + \mu_t \left[\left(\frac{\partial u}{\partial x}\right)^2 + \left(\frac{\partial u}{\partial y}\right)^2\right] - \rho\varepsilon = 0, \tag{3}$$

where $\mu_k = \mu + \mu_t/\sigma_k$.

In the outer region, the length scale ℓ_μ is given as

$$\ell_\mu = \frac{k^{3/2}}{\varepsilon}, \tag{4}$$

and the dissipation rate, ε, is found from the model equation

$$\frac{\partial}{\partial x}\left(\mu_\varepsilon \frac{\partial \varepsilon}{\partial x}\right) + \frac{\partial}{\partial y}\left(\mu_\varepsilon \frac{\partial \varepsilon}{\partial y}\right) + C_{1\varepsilon}\frac{\varepsilon}{k}\mu_t \left[\left(\frac{\partial u}{\partial x}\right)^2 + \left(\frac{\partial u}{\partial y}\right)^2\right] - C_{2\varepsilon}\rho\frac{\varepsilon^2}{k} = 0, \tag{5}$$

where $\mu_\varepsilon = \mu + \mu_t/\sigma_\varepsilon$.

In the inner region, the turbulence length scale takes the form as proposed by Wolfshtein (1969),

$$\ell_\mu = C_\ell d_{\text{eff}}\left(1 - \mathrm{e}^{-R_k/A_\mu}\right), \tag{6}$$

and the dissipation rate is represented by

$$\varepsilon = \frac{k^{3/2}}{\ell_\varepsilon}, \tag{7}$$

Table 1
Values for the turbulence model coefficients

C_μ	A_μ	A_ε	κ	$C_{1\varepsilon}$	$C_{2\varepsilon}$	σ_k	σ_ε
0.09	70.0	5.08	0.418	1.44	1.92	1.0	1.3

where the length scale ℓ_ε is given as

$$\ell_\varepsilon = C_\ell d_{\text{eff}}\left(1 - \mathrm{e}^{-R_k/A_\varepsilon}\right).$$

The parameter $R_k = \rho\sqrt{k}d_{\text{eff}}/\mu$ is a wall-distance Reynolds number in which, for smooth surfaces, d_{eff} is the shortest distance, d, to a surface, either the wall or the interface. The parameters in the turbulence model are chosen in accordance with Chen and Patel (1988), and their values are summarized in Table 1. They selected the constant C_ℓ equal to $\kappa/C_\mu^{3/4}$ in order to match the log-layer solution, where κ is the von Karman constant. The model coefficient $A_\mu = 70$ was assigned so that the model recovers the additive constant in the logarithmic law. Also, Chen and Patel (1988) used $A_\varepsilon = 2C_\ell$ to obtain the proper asymptotic behaviour $\varepsilon \to 2k\mu/\rho d^2$ as $d \to 0$.

The two-layer formulation consists simply of using Eqs. (6) and (7) near physical boundaries, and switching abruptly to Eqs. (4) and (5) at a matching point where viscous effects become negligible. Chen and Patel (1988) suggested $R_k = 250$ as a suitable matching criterion. At this point the damping function $(1 - \mathrm{e}^{-R_k/A_\mu})$ takes a value of 0.97, approximately. The same criterion has been adopted here to match the two models.

It should be noticed that secondary flows are known to appear in non-circular ducts (Demuren and Rodi, 1984), and it can also be observed in stratified gas–liquid pipe flow (e.g. Strand, 1993). The effect of secondary motions produces a downward shift in the location of the maximum in the gas velocity profile (Meknassi et al., 2000). But, modelling this phenomenon would require calculations of all the Reynolds stresses, involving more sophisticated turbulence models. This will lead to a significant increase in computational cost for what is expected to be only a marginal increase in predictability (Newton and Behnia, 2000); consequently, it is neglected in this study.

2.3. Modification for interfacial waves

The concept of representing the interfacial waves as surface roughness requires modifications to the turbulence model described above. In general, roughness has the effect of disrupting the viscous sublayer, leading to a shift in the logarithmic velocity profile:

$$u^+ = \frac{1}{\kappa}\ln d^+ + B + \Delta B_{\text{s}}(R_{\text{s}}^+),$$

where u^+ and d^+ are the normalised velocity and distance, respectively, based on the local friction velocity $u_\tau = \sqrt{\tau/\rho}$ for surface shear stress τ. The normalised roughness height, $R_{\text{s}}^+ = \rho R_{\text{s}} u_\tau/\mu$, is based on an *equivalent sand-grain roughness height*, R_{s}. The function ΔB_{s} represents the alteration of the additive constant, B, by roughness. Nikuradse (1933) measured this roughness function experimentally and Ligrani and Moffat (1986) fit the curve

$$\Delta B_{\text{s}} = \begin{cases} 0, & \text{for } R_{\text{s}}^+ < 2.25, \\ (8.5 - B - \frac{1}{\kappa}\ln R_{\text{s}}^+)\sin\left[\frac{\pi/2\ln(R_{\text{s}}^+/2.25)}{\ln(90/2.25)}\right], & \text{for } 2.25 \leqslant R_{\text{s}}^+ \leqslant 90, \\ 8.5 - B - \frac{1}{\kappa}\ln R_{\text{s}}^+, & \text{for } R_{\text{s}}^+ > 90, \end{cases}$$

through his experiments. Consequently, the rough-surface turbulent flow is divided into three regimes: hydraulically smooth ($R_{\text{s}}^+ < 2.25$), transitionally rough ($2.25 \leqslant R_{\text{s}}^+ \leqslant 90$), and fully rough ($R_{\text{s}}^+ > 90$). The parameter R_{s}^+ is introduced as a means of converting roughness data obtained

from other roughness types and other flow configurations into a roughness measure equivalent to the measurements of Nikuradse (1933).

The shift in the logarithmic profile is due to the increased drag force exerted by the rough surface on the flow. This increased flow resistance can be modelled by displacing the effective position of the surface by the *displacement height* Δd (Rotta, 1962), which artificially increases the turbulent length scale, and thereby increases the shear stress near the rough surface. Patel and Yoon (1995) adopted this modification to their two-layer turbulence model and defined the effective distance, d_{eff}, to a rough surface as

$$d_{\text{eff}} = d + \Delta d.$$

The normalised displacement height, $\Delta d^+ = \rho \Delta d u_\tau / \mu$, was expressed as a function of the equivalent roughness parameter R_{s}^+ (Cebeci and Smith, 1974),

$$\Delta d^+ = 0.9\left(\sqrt{R_{\text{s}}^+} - R_{\text{s}}^+ \mathrm{e}^{-R_{\text{s}}^+/6}\right). \tag{8}$$

This relation is a curve fit to the correlation of Rotta (1962), and it is valid for $4.535 < R_{\text{s}}^+ < 2000$. The lower bound corresponds to hydraulically smooth surfaces, where $\Delta d^+ \cong 0$.

A similar analogy can be used for wavy gas–liquid flows, where the flow resistance is increased because of the interfacial waves. In order to take this effect into account, the effective distance in the turbulence model can be increased on both sides of the interface by the displacement height Δd_ϕ.

Assuming that the interfacial roughness R_{s} is known, the equivalent interfacial roughness parameter on both sides of the interface is given by $R_{\text{s}}^+ = \rho R_{\text{s}} u_{\tau,\text{i}} / \mu$, where the interfacial friction velocity, $u_{\tau,\text{i}} = (\bar{\tau}_{\text{i}}/\rho)^{1/2}$, is based on the average interfacial shear stress $\bar{\tau}_{\text{i}}$. Further, the normalised displacement height Δd_ϕ^+ can be calculated using Eq. (8), and Δd_ϕ is then given by $\mu \Delta d_\phi^+ / \rho u_{\tau,\text{i}}$. This displacement height will take a different value in the gas phase and the liquid phase due to the difference in density and viscosity.

In the present approach, the turbulence is completely damped towards the pipe wall. This means that the effective distance in the turbulence model is chosen as the shortest distance to the wall or the interface, where the distance to the interface is increased by the displacement height, i.e.

$$d_{\text{eff}} = \min(d_{\text{w}}, d_\phi + \Delta d_\phi).$$

This way, the turbulence in the vicinity of the interface is not fully damped, leading to an increase in the interfacial shear stress and, hence, flow resistance. How to obtain the interfacial roughness is discussed in Section 3.2.

Durbin et al. (2001) found it necessary to also delete the damping of the turbulent viscosity to accommodate the fully rough conditions. They suggested the simple linear interpolation

$$A_\mu = \max\left[A_\mu^{\min}, A_\mu^0(1 - R_{\text{s}}^+/90)\right],$$

where A_μ^0 is the value for the smooth case ($A_\mu^0 = 70$) and $A_\mu^{\min}$ was set equal to one. A similar approach for the wavy gas–liquid flow was found to introduce too much turbulent diffusion in both phases. Instead, the turbulence damping near the interface was reduced in the liquid phase only. The expression above was used, where $A_\mu^{\min}$ was conveniently chosen as 20.

2.4. Boundary conditions

In the early work of Akai et al. (1981) it was suggested that the continuity condition for the turbulent kinetic energy was not always necessary. They explained this by the large scale eddies containing a large amount of energy produced by the flow separation in the gas phase. This is not considered to be a concern in the liquid phase. The same argument was used by Newton and Behnia (2001), who used the boundary condition for k on a fully rough surface, $\tau/\rho\sqrt{C_\mu}$, at the interface. Since the interfacial shear stress is continuous, the level of k at the interface will differ by the ratio of the fluid densities.

A similar boundary condition is used in this study for a fully rough interface, whereas a simple quadratic interpolation (Durbin et al., 2001) is adopted for the transitional regime. The interfacial boundary condition for k takes the form

$$k_{\mathrm{i,L}} = \frac{\hat{\tau}_\mathrm{i}}{\rho_\mathrm{L}\sqrt{C_\mu}} \min\left[1, (R_\mathrm{s}^+/90)^2\right] \quad \text{and} \quad k_{\mathrm{i,G}} = \frac{\hat{\tau}_\mathrm{i}}{\rho_\mathrm{G}\sqrt{C_\mu}} \min\left[1, (R_\mathrm{s}^+/90)^2\right] \tag{9}$$

in the liquid and gas phase, respectively.

In this approach, the local interfacial shear stress, $\hat{\tau}_\mathrm{i}$, is given by the following power law distribution of the average shear stress (Newton and Behnia, 2001)

$$\hat{\tau}_\mathrm{i} = \left(1 + \frac{1}{m}\right)\bar{\tau}_\mathrm{i}\left(1 - \frac{s}{c}\right)^{1/m}, \tag{10}$$

where $m = 6.6$, c is half the width of the interface (see Fig. 1), and s is the distance from the vertical centerline along the interface. This empirical distribution ensures that the level of turbulence will be reduced close to the wall, and the maximum value for k_i will be at the vertical centerline of the pipe. The average interfacial shear stress, $\bar{\tau}_\mathrm{i}$, is estimated from the flow field.

For the gas flow it is generally accepted that the interface acts like a wall; hence, the boundary condition (9) seems physically reasonable. The choice of interfacial value for k may not be that clear for the liquid phase. Based on different physical arguments, a number of investigators have suggested various interfacial boundary conditions in the liquid flow (e.g. Akai et al., 1981; Lorencez et al., 1997; Meknassi et al., 2000; Newton and Behnia, 2001); nevertheless, none of these seem to be as widely accepted as the interfacial boundary condition on the gas side. In this work, the choice is merely based on the successful use by Newton and Behnia (2001) for wavy gas–liquid flow in pipes.

The velocity field, which provides the only coupling between the phases, is continuous at the interface,

$$u_{\mathrm{i,L}} = u_{\mathrm{i,G}}.$$

For the non-smooth case, the turbulent viscosity takes a non-zero value at the interface, and the requirement of continuity in shear stress yields the following interfacial boundary condition

$$(\mu + \mu_{t,\mathrm{i}})_\mathrm{L}\frac{\partial u_{\mathrm{i,L}}}{\partial n} = (\mu + \mu_{t,\mathrm{i}})_\mathrm{G}\frac{\partial u_{\mathrm{i,G}}}{\partial n}.$$

At the pipe wall, the no-slip condition yields the following boundary conditions for velocity and turbulent kinetic energy

$$u_w = 0 \quad \text{and} \quad k_w = 0,$$

where the subscript w denotes the boundary value at the wall.

In the near-wall and near-interface regions, the turbulent viscosity and dissipation rate are expressed explicitly by Eqs. (2) and (7), respectively. Therefore, no boundary conditions are required for μ_t and ε, neither at the wall nor interface.

2.5. Numerical method

A finite difference scheme is used to discretize the governing Eqs. (1), (3) and (5). The numerical grid consists of a composite, overlapping grid (Chesshire and Henshaw, 1990) where a local grid refinement technique (Martin and Cartwright, 1996) is adopted to adequately resolve the large variations of the turbulent quantities near the wall and the interface (see Fig. 2).

The idea behind a composite grid framework is to divide a complex computational domain into simpler subdomains, so that every subdomain can be covered with a component grid. The component grids may overlap in order to cover the entire computational domain. Each component grid is logically rectangular, and it has its own coordinate transformation,

$$(x, y) = \Phi(\xi, \eta),$$

from the computational space (ξ, η) to the physical space (x, y). Every point on a component grid are classified as one of the following: *Discretization point* (active grid cell), *interpolation point* (inactive grid cell) or *unused point*. Grid function values at interpolation points of a component grid are obtained by two-dimensional quadratic interpolation from discretization points on an-

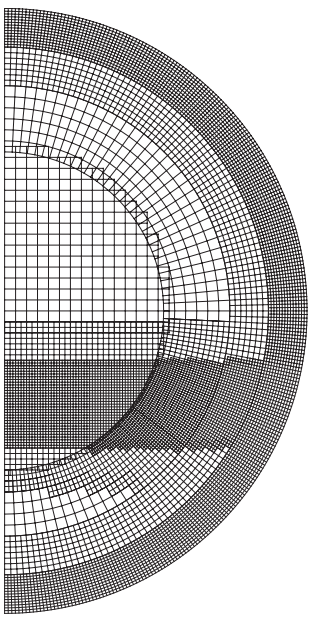

Fig. 2. The composite overlapping grid with local grid refinement near the pipe wall and near the interface. The figure shows only the active grid cells.

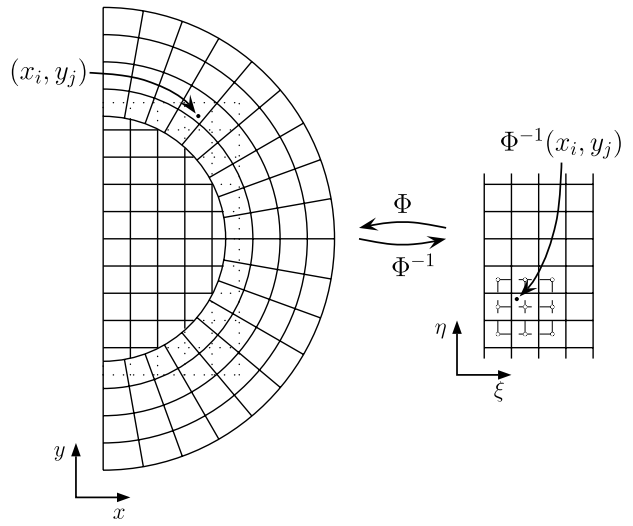

Fig. 3. Interpolation points in computational space for coupling between overlapping composite grids.

other component grid. The interpolation is done in the computational space using standard interpolation techniques (see Fig. 3).

The grid is refined by adding block-structured subgrids to regions with large variations. These refined subgrids use information from coarser grid levels by updating the boundary cells using higher order interpolation. Information from refined levels is passed to the coarser level using the *refined flux* at the coarse/fine interface. The discrete equations are solved iteratively and separately on each subgrid. Interior boundary cells are updated as information is passed between the grids after every iteration step.

The immersed interface method is used to treat the interfacial boundary conditions properly. The decomposed approach of Berthelsen (2004a) is used here, where componentwise correction terms are added to the standard finite difference stencil to make the discretization well-defined across the interface at any position regardless of the grid.

Further details about the numerical procedure can be found in the references above and in the thesis of Berthelsen (2004b).

3. Results and discussion

3.1. Experimental data

Numerical results for stratified wavy flow are compared with the measurements from Espedal's (1998) experiments where the pipe was inclined upwards with the inclination angle $\theta = 0.104°$. Espedal (1998) measured liquid holdup, pressure gradient and wall shear stress for stratified air-water flow in a 0.06 m diameter pipe for a large number of combinations of air and water rates. The interface was characterized as wavy with large 3D waves in the data chosen for evaluation of the model.

Although (as demonstrated by Berthelsen and Ytrehus, 2004, 2005) the method is capable of resolving stratified flow with a pre-defined curved interface, the calculations presented here assumes a flat interface, basically, since no information about the interface shape is given in the experimental data. This assumption is not far from realistic since the gravitational force dominates the surface tension force in most practical gas–liquid flows.

3.2. Estimating the interfacial roughness

Following Meknassi et al. (2000), the equivalent roughness height of the interface can be estimated for a given experimental estimation of the friction factor using a classical relationship between friction factor and roughness in turbulent flow. Meknassi et al. (2000) compared this method of obtaining the roughness with the value determined from the experimental profile of longitudinal velocity above the waves using the experimental data of Strand (1993). They concluded that the values were very close.

Using Colebrook's (1939) equation, the equivalent roughness has been estimated from Espedal's (1998) data. The normalised roughness height based on the gas flow is plotted as a function of the gas superficial velocity in Fig. 4. The plot show a similar trend to the results obtained by Meknassi et al. (2000) for Strand's (1993) data, where low gas superficial velocity yields roughness below the fully rough regime.

According to Charnock (1955), the surface roughness was linked to the frictional velocity by the following expression:

$$R_s = \beta \frac{u_{\tau,i}^2}{g},$$

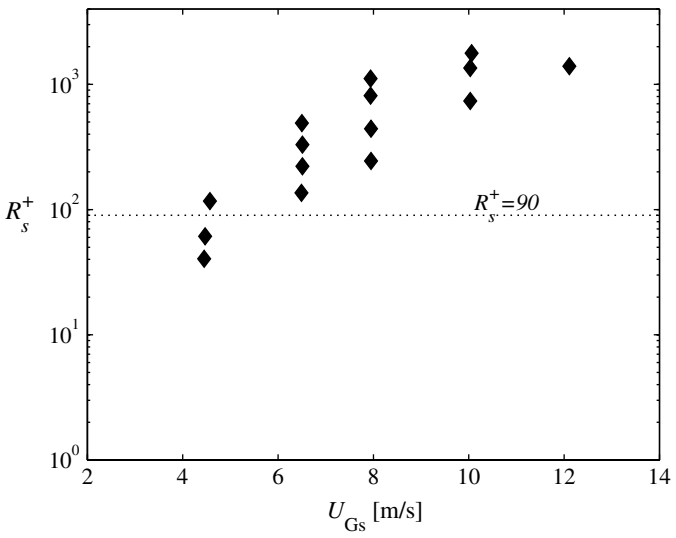

Fig. 4. Normalised roughness versus gas superficial velocity after Espedal's data for upward inclined pipes with inclination angle $\theta = 0.104°$.

where the parameter β is between 0.36 and 1.05 for deep water waves. Rosant (1983) proposed to modify β for pipe flow as follows:

$$\beta = 1238\left(\frac{\rho_G}{\rho_L}\right)\min(H_L, 0.1),$$

where H_L is the liquid phase area fraction, often referred to as the liquid holdup. The data presented in Fig. 5 gave a wide scattered result for the parameter β, ranging from 0.1 to 0.2, and Rosant's (1983) correlation will in most cases give a too low estimate of the Charnock roughness parameter for the data presented here. On the other hand, correlating β with the liquid superficial velocity, U_{Ls}, seem to give a less scattered result, as shown in Fig. 6, for the current data. The linear fit

$$\beta = A + BU_{Ls}, \tag{11}$$

where $A = 0.0866$ and $B = 2.18$ s/m, is used as an approximation to β in the numerical results presented herein.

3.3. Pressure gradient and liquid holdup

The pressure gradient and liquid holdup can be determined by imposing the gas and liquid flow rates in the numerical simulations. Predicted pressure gradient and liquid holdup as functions of the liquid superficial velocity are compared with the experimental data in Figs. 7 and 8, respectively, for $U_{Gs} = 6.5$ m/s and $U_{Gs} = 8.0$ m/s. The plots also include numerical predictions obtained by assuming a smooth interface to illustrate the effect of interfacial waves on global flow properties.

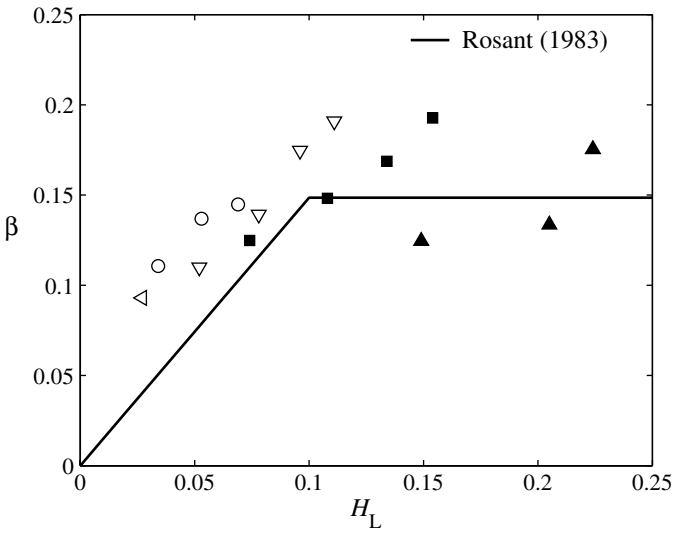

Fig. 5. Charnock type roughness parameter versus liquid holdup for upward inclined pipes with inclination angle $\theta = 0.104°$: (▲) $U_{Gs} = 4.5$ m/s; (■) $U_{Gs} = 6.5$ m/s; (∇) $U_{Gs} = 8.0$ m/s; (○) $U_{Gs} = 10.0$ m/s; (◁) $U_{Gs} = 12.0$ m/s.

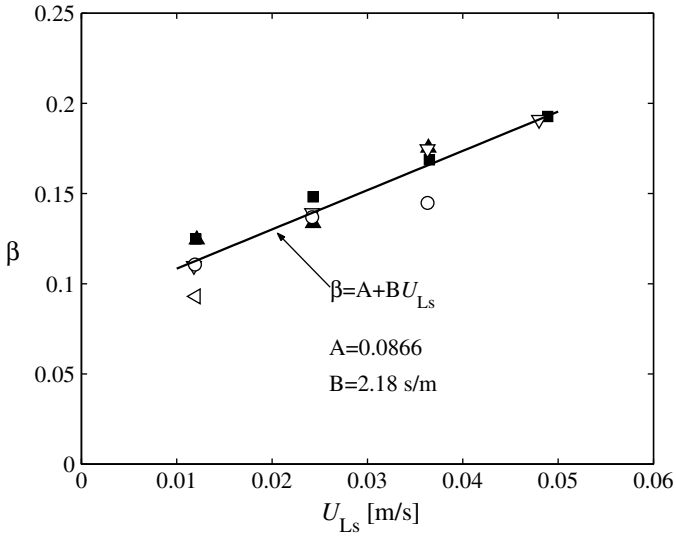

Fig. 6. Charnock type roughness parameter versus liquid superficial velocity for upward inclined pipes with inclination angle $\theta = 0.104°$ (symbol refer to Fig. 5).

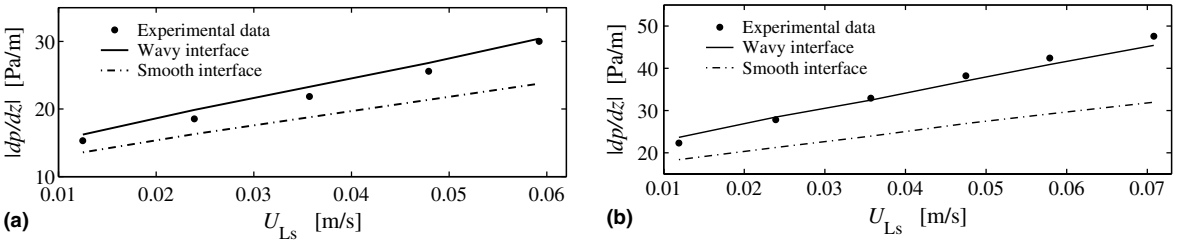

Fig. 7. Calculated axial pressure gradient compared with experimental results: (a) $U_{Gs} = 6.5$ m/s; (b) $U_{Gs} = 8.0$ m/s. Inclination angle $\theta = 0.104°$.

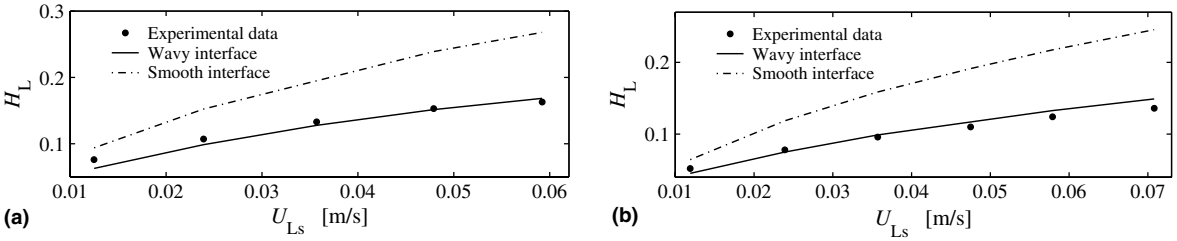

Fig. 8. Calculated liquid holdup compared with experimental results: (a) $U_{Gs} = 6.5$ m/s; (b) $U_{Gs} = 8.0$ m/s. Inclination angle $\theta = 0.104°$.

The interfacial friction increases for a wavy interface, which gives higher flow resistance, and a larger pressure gradient is necessary to maintain the same flow rates. Including a rough interface

into the model gives higher values for the pressure gradient than obtained when assuming a smooth interface, and the calculated values agrees better with the experimental data. The liquid holdup predicted with a rough interface compares well with the measurements, while the result obtained with a smooth interface over-predicts the holdup noticeable. The increased interfacial friction causes the liquid phase to move faster due to the larger dragging effect from the gas phase; thus, the liquid holdup must decrease in order to maintain the same liquid flow rate.

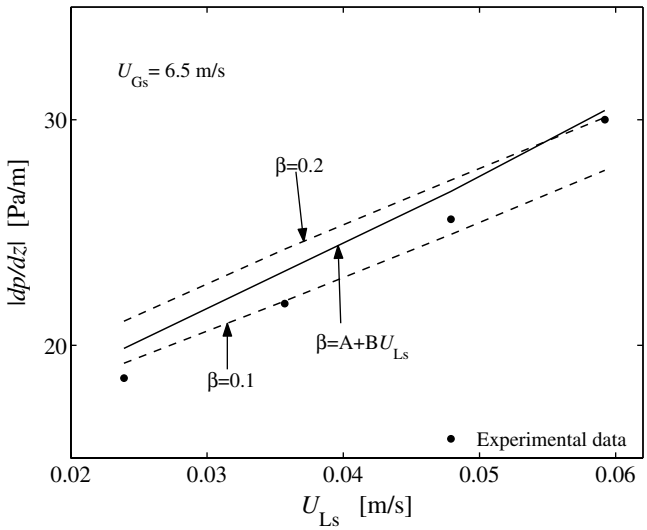

Fig. 9. Sensitivity of calculated pressure gradient to the Charnock parameter. Inclination angle $\theta = 0.104°$.

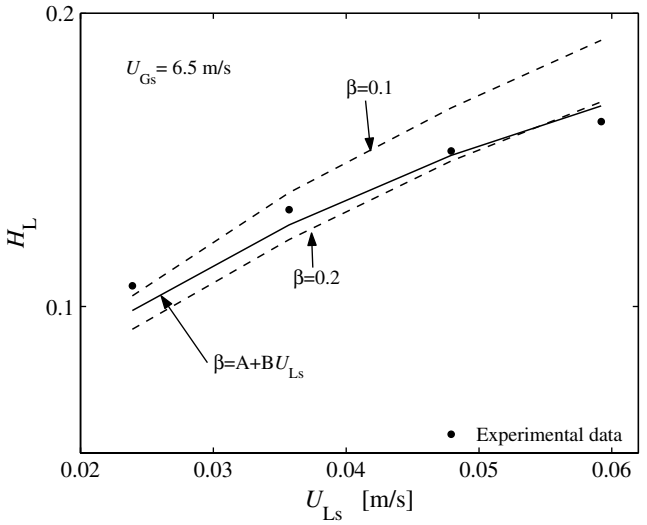

Fig. 10. Sensitivity of calculated liquid holdup to the Charnock parameter. Inclination angle $\theta = 0.104°$.

The sensitivity of the numerical results to the Charnock parameter is shown in Figs. 9 and 10 for the pressure gradient and the liquid holdup, respectively. It is clear that the choice of Charnock parameter has an effect on the calculated results; however, this effect is not too dramatic. On average, doubling the Charnock parameter from $\beta = 0.1$ to $\beta = 0.2$ leads to an increase in the calculated pressure gradient of only 9.5% and a decrease of 11% in the calculated liquid holdup.

Figs. 9 and 10 suggest that using a lower value for β than given by Eq. (11) should improve the calculations when $U_{Ls} < 5$ m/s, but, according to Fig. 6, β should be larger to fit the experimental estimates of the Charnock parameter better for the current cases. It may seem like Colebrook's (1939) equation provides too large estimates of the equivalent interfacial roughness height for low liquid flow rates, but as will be pointed out in the next section, there is more likely to be other explanations to the discrepancy in the results.

Despite the uncertainties related to using the Charnock parameter, treating the wavy interface as a rough surface gives significant improvements of the results. The average error obtained with the present approach is approximately 7% in estimating the liquid holdup and 4% in predicting the pressure gradient, while similar results obtained when assuming a smooth interface yields as much as 56% in average error in estimating the liquid holdup and 22% when calculating the pressure gradient.

3.4. Shear stress

Espedal (1998) conducted wall shear stress measurements for similar flow conditions as in his pressure gradient and liquid holdup experiments. These measurements are used to evaluate the performance of the present model. Numerical estimates of the shear stress are obtained by imposing the pressure gradient and liquid holdup in the simulation. The results are compared with experimental data in Table 2 for average values, and it should be noted that the difference in the experimental flow rates and the flow rates calculated in these simulations are less than 6%. The experimental data for the average liquid wall shear stress and the average interfacial shear stress are obtained from a momentum balance using the measured gas wall shear stress, pressure gradient and liquid holdup.

A wavy interface increases the interfacial shear stress, which transfer momentum from the gas phase into the liquid phase, leading to a decrease in the gas wall shear stress and an increase in the liquid wall shear stress. Fig. 11 illustrates this, where the calculated wall shear stress distributions

Table 2
Comparison of experimental (exp) shear stresses and calculated (cal) shear stresses

U_{Gs} [m/s]		U_{Ls} [m/s]		$\bar{\tau}_G$ [Pa]		$\bar{\tau}_L$ [Pa]		$\bar{\tau}_i$ [Pa]	
(exp)	(cal)	(exp)	(cal)	(exp)	(cal)	(exp)	(cal)	(exp)	(cal)
6.51	6.21	0.0243	0.0250	0.207	0.205	0.401	0.382	0.444	0.428
6.51	6.20	0.0365	0.0362	0.220	0.222	0.491	0.470	0.531	0.499
6.50	6.26	0.0489	0.0474	0.234	0.241	0.600	0.569	0.633	0.590
7.95	7.71	0.0242	0.0240	0.277	0.284	0.711	0.664	0.733	0.673
7.94	7.94	0.0363	0.0347	0.296	0.318	0.929	0.832	0.944	0.830
7.94	8.09	0.0480	0.0451	0.315	0.346	1.09	0.979	1.09	0.964

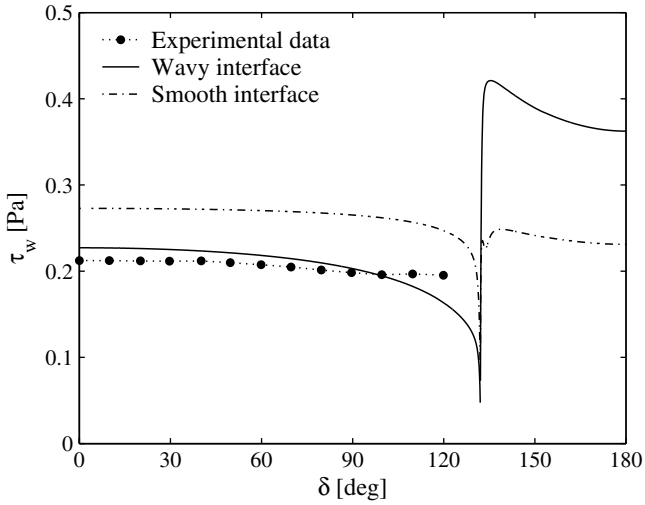

Fig. 11. Comparison of predicted and measured angular distribution of wall shear stress for $dp/dz = 19.2$ Pa/m and $H_L = 0.108$. $\delta = 0°$ at the top of the pipe. Inclination angle $\theta = 0.104°$.

for both a rough and a smooth interface are compared with the measured distribution in the gas phase. Including a rough interface in the model decreases the estimated gas wall shear stress and increases the estimated wall shear stress in the liquid phase as compared to the simulation with a smooth interface. The predicted wall shear stress distribution compares quite well with the experimental data, except in the vicinity of the gas–liquid interface. The integral of the shear stress around the circumference should exactly balance the axial pressure force and gravity force, regardless of whether the interface is smooth or wavy. This means that the integral of the shear stress should be the same for a wavy and a smooth interface, and, as illustrated in Fig. 11, the

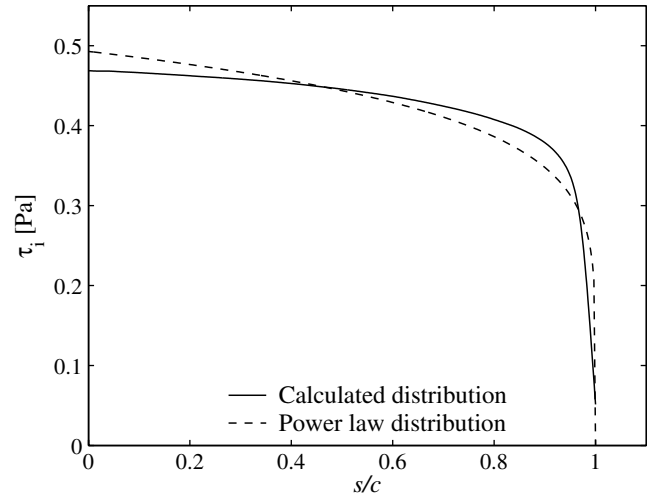

Fig. 12. Comparison of calculated interfacial shear stress distribution and the power law relation given by Eq. (10) for $dp/dz = 19.2$ Pa/m and $H_L = 0.108$. Inclination angle $\theta = 0.104°$.

difference is negligible small (about 1%). The calculated interfacial shear stress distribution is compared with the power law distribution defined by Eq. (10) in Fig. 12. The power law relation gives a fair approximation of the distribution.

It can be observed in Table 2 that the error in predicting the average shear stresses increases for increasing flow rates. In general, the present model fails to increase the interfacial shear stress sufficiently to transport enough energy from the gas phase to the liquid phase; hence, the gas wall shear stress is slightly over-predicted and the liquid wall shear stress is slightly under-predicted. Although the deviation in the interfacial shear stress is as large as 7% for $U_{Gs} = 6.5$ m/s and 12% for $U_{Gs} = 8.0$ m/s, the error is considered to be satisfactory for a quantity like interfacial shear stress for wavy interfaces. Similar conclusion can be made for the wall shear stresses.

Since the momentum transfer from the gas phase to the liquid phase is under-predicted, it is expected that the calculated gas flow rate would exceed the measured flow rate for given pressure gradient and liquid holdup. Evidently, this is not the case for the lowest flow rates. This suggest that the present approach introduces too much turbulent viscosity in the gas phase further away from the wavy interface, although the increased turbulent viscosity at the interface is not sufficiently large. It was shown in the previous section that using a lower value for the Charnock parameter than given by Eq. (11) would improve the predictions of pressure gradient and liquid holdup at low liquid flow rates. But, the Charnock parameter needs to be larger in order to increase the interfacial roughness, and hence, to increase the interfacial shear stress through the increased displacement height Δd_ϕ. Therefore, as pointed out by Newton and Behnia (2001), the boundary condition on the turbulent kinetic energy on the gas side of the interface may be too high, leading to too much turbulent viscosity in the gas phase. Unfortunately, the available experimental information does not allow for a conclusion at this point.

3.5. Flow field

Fig. 13 shows the calculated velocity fields when assuming a rough and a smooth interface. The pressure gradient and liquid holdup are equal for both cases. The interfacial roughness increases

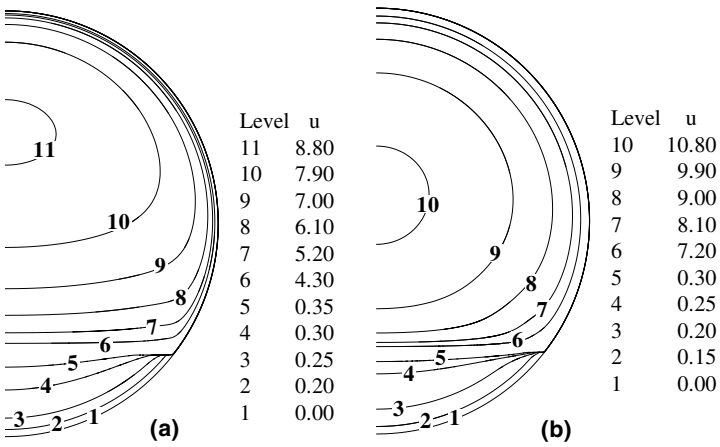

Fig. 13. Calculated velocity field for $dp/dz = 22.3$ Pa/m and $H_L = 0.134$, contours in m/s: (a) wavy interface; (b) smooth interface. Inclination angle $\theta = 0.104°$.

the flow resistance near the interface; consequently, the gas flow rate is decreased, and the maximum in the gas velocity profile is shifted upwards. The turbulence generated by the rough interface clearly increases the level of turbulent kinetic energy in both phases, as shown in Fig. 14, particularly near the interface region. Also, vertical profiles of u, k and ε are given in Figs. 15–17.

There is a clear distinction in the behaviour of the momentum correction factor for a rough and a smooth interface (see Fig. 18). The momentum correction factor measures the deviation of the velocity profile from the mean value and is defined as

$$\mathrm{MCF}_q = \frac{\int_{A_q} u(x,y)^2 \,\mathrm{d}A}{\bar{u}_q^2 A_q} \quad \text{for } q = (\mathrm{G},\ \mathrm{L}),$$

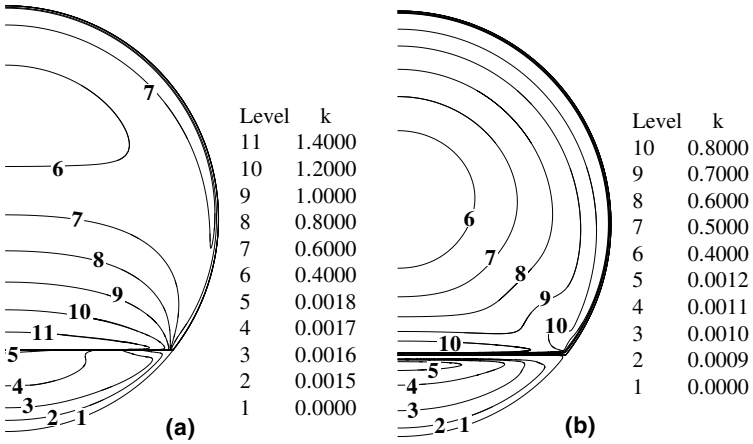

Fig. 14. Calculated distribution of turbulent kinetic energy for $\mathrm{d}p/\mathrm{d}z = 22.3$ Pa/m and $H_\mathrm{L} = 0.134$, contours in $\mathrm{m}^2/\mathrm{s}^2$: (a) wavy interface; (b) smooth interface. Inclination angle $\theta = 0.104°$.

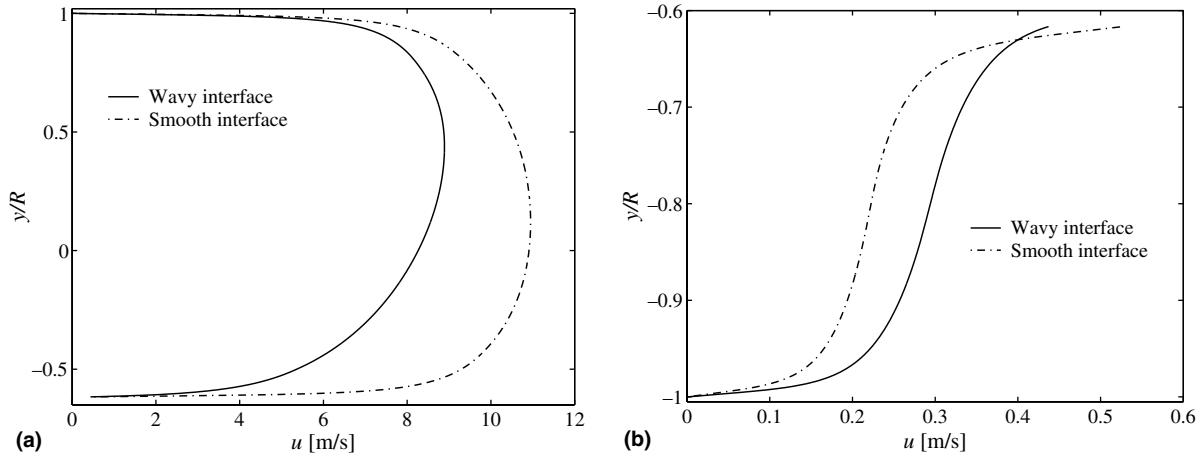

Fig. 15. Calculated vertical centerline velocity profile for wavy and smooth interface, $\mathrm{d}p/\mathrm{d}z = 22.3$ Pa/m and $H_\mathrm{L} = 0.134$: (a) gas phase; (b) liquid phase. Inclination angle $\theta = 0.104°$.

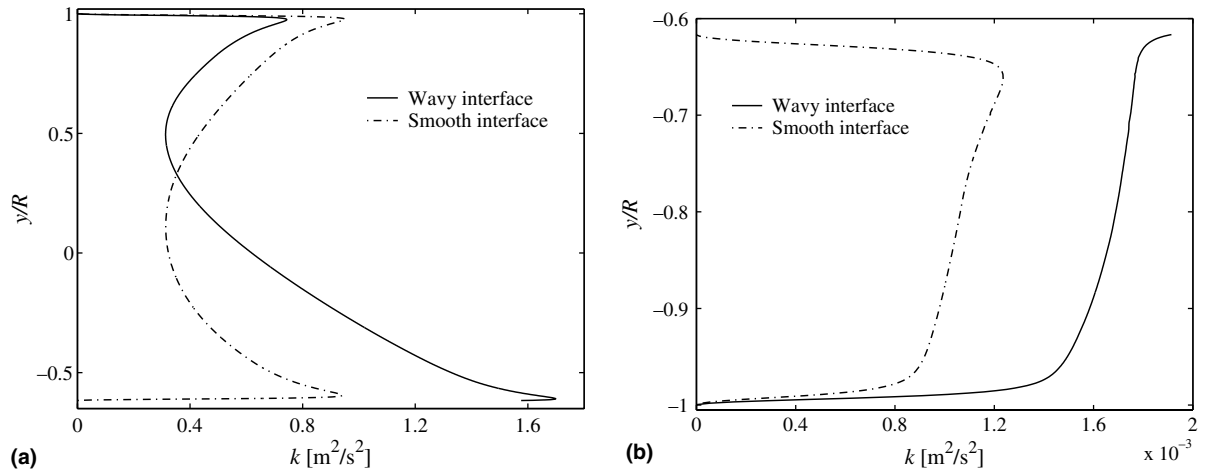

Fig. 16. Calculated vertical centerline profile of turbulent kinetic energy for wavy and smooth interface, $dp/dz = 22.3$ Pa/m and $H_L = 0.134$: (a) gas phase; (b) liquid phase. Inclination angle $\theta = 0.104°$.

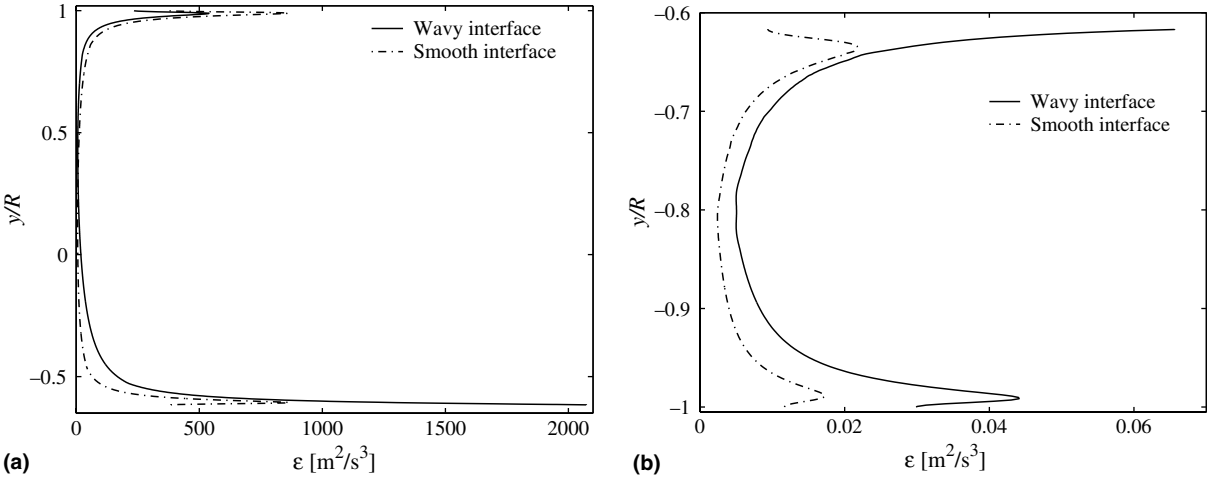

Fig. 17. Calculated vertical centerline dissipation rate profile for wavy and smooth interface, $dp/dz = 22.3$ Pa/m and $H_L = 0.134$: (a) gas phase; (b) liquid phase. Inclination angle $\theta = 0.104°$.

where the area-averaged velocity in phase q is denoted $\bar{u}_q$ and A_q is the phase cross-sectional area. For a smooth interface, the gas velocity profile is rather symmetric and flat, yielding a nearly constant value close to unity for the momentum correction factor. The rough interface causes a deviation from this symmetric profile, as seen in Fig. 15, leading to an increase in the momentum correction factor. This effect becomes more pronounced for increased gas velocity. On the other hand, the increased turbulent viscosity in the liquid phase results in a flatter liquid velocity profile; hence, the momentum correction factor decreases as compared to the smooth interface where turbulence is damped towards the interface creating a laminar zone.

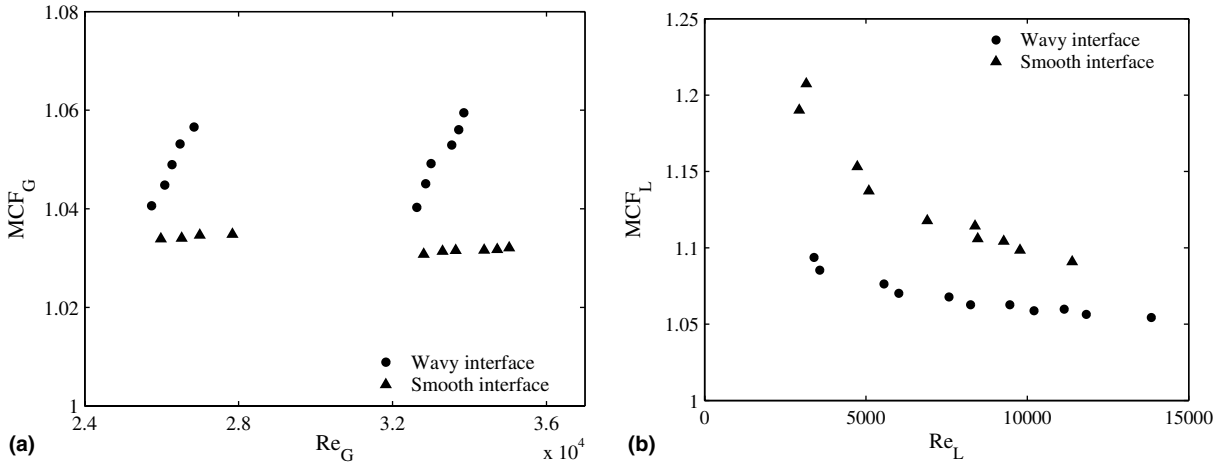

Fig. 18. Calculated momentum correction factors for wavy and smooth interface: (a) gas phase; (b) liquid phase. Inclination angle $\theta = 0.104°$.

Espedal (1998) did not perform measurements of velocity profiles in his experiments; instead, the present method is compared with the experimental data provided by Newton and Behnia (2001). Fig. 19 presents a comparison between calculated and measured velocity profiles in a horizontal pipe where the flow rates have been imposed in the numerical calculations. The graph shows numerical results for both smooth and rough interfaces, where the Charnock parameter, β, is chosen as 0.25 for the cases with a rough interface. It can be observed that the present approach with rough interface compares reasonably well with the experimental data. The increased flow resistance near the wavy interface in the gas phase shifts the location of the maximum velocity upwards, and the predicted profiles captures this trend when the interface is treated as a rough

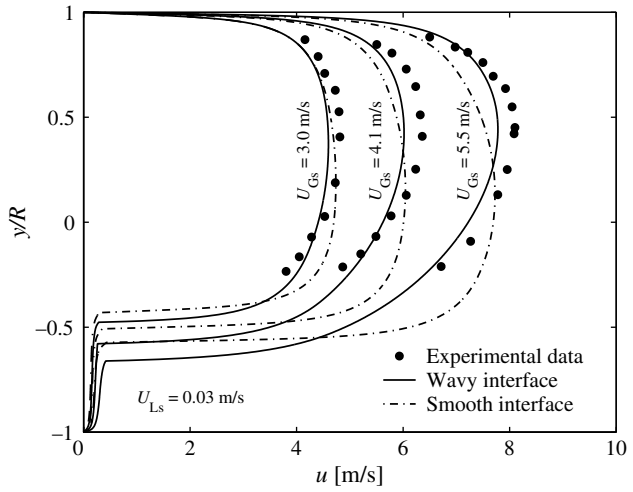

Fig. 19. Comparison of calculated and measured centerline velocity profiles for flow in horizontal pipes. The experimental data is taken from Newton and Behnia (2001). $\beta = 0.25$ for the calculations with a wavy interface.

surface. It is believed that the present approach may under-predict the liquid holdup since the level of turbulence in the gas phase is too high; therefore, the predicted velocity profiles in the gas phase in Fig. 19 yield lower mean values than the experimental data.

4. Concluding remarks

A method for the calculation of fully developed, stratified wavy two-phase flow in pipes has been developed, where the wavy interface is represented by an equivalent interfacial roughness. Turbulent stresses were modelled using a two-layer turbulence model, which has been modified to account for the roughness introduced at the interface.

Numerical calculations of global properties, such as pressure gradient and liquid holdup, have been compared with the experimental data of Espedal (1998). The results showed acceptable agreement with the measurements. Calculated wall and interfacial shear stresses were also found to compare satisfactorily with the experiments. The interfacial roughness, represented by the Charnock parameter, was estimated from Espedal's experiments. The results were sensitive to the choice of Charnock parameter, but not too dramatic as a large change in the Charnock parameter only led to a small difference in the calculation. The level of turbulent kinetic energy is found to be slightly over-predicted in the gas phase, and, as pointed out by others, it is suggested that the interfacial boundary value for the turbulent kinetic energy may be too high on the gas side. In addition, numerical results have been compared with the measured velocity profiles presented by Newton and Behnia (2001). The agreement between the calculated and measured profiles seems reasonable.

In principle, there are two ways the present method differs from previous studies of two-dimensional modelling of stratified wavy pipe flow. Firstly, it utilises the immersed interface method in order to treat interfacial boundary conditions numerically, and, as shown by Berthelsen and Ytrehus (2004, 2005), extension to arbitrary shaped interfaces or three-phase flow is rather straight forward. Secondly, the use of a two-layer turbulence model with an interfacial roughness formulation provides for direct evaluation of the interfacial shear stress without of the use of wall functions. The interfacial shear stress is a result of the calculation and not imposed on the numerical scheme as done by some others.

Acknowledgments

This work was supported by the Norwegian Research Council through the Petronics programme.

References

Agrawal, S.S., Gregory, G.A., Govier, G.W., 1973. An analysis of horizontal stratified two phase flow in pipes. Can. J. Chem. Eng. 51, 280–286.

Akai, M., Inoue, A., Aoki, S., Endo, K., 1980. A co-current stratified air-mercury flow with wavy interface. Int. J. Multiphase Flow 6, 173–190.

Akai, M., Inoue, A., Aoki, S., 1981. The prediction of stratified two-phase flow with a two-equation model of turbulence. Int. J. Multiphase Flow 7, 21–39.

Andreussi, P., Persen, L.N., 1987. Stratified gas–liquid flow in downwardly inclined pipes. Int. J. Multiphase Flow 13, 565–575.

Andritsos, N., Hanratty, T.J., 1987. Influence of interfacial waves in stratified gas–liquid flows. AIChE J. 33, 444–454.

Berthelsen, P.A., 2004a. A decomposed immersed interface method for variable coefficient elliptic equations with non-smooth and discontinuous solutions. J. Comput. Phys. 197, 364–386.

Berthelsen, P.A., 2004b. An immersed interface method for two-dimensional modelling of stratified flow in pipes. Ph.D. thesis, Norwegian University of Science and Technology, Department of Energy and Process Engineering, Trondheim, Norway. Available from: <http://www.diva-portal.org/ntnu/theses/abstract.xsql?dbid=306>.

Berthelsen, P.A., Ytrehus, T., 2004. Numerical modelling of stratified turbulent two- and three-phase pipe flow with arbitrary shaped interfaces. The 5th International Conference on Multiphase Flow, ICMF'04, Yokohama, Japan, May 30–June 4.

Berthelsen, P.A., Ytrehus, T., 2005. Stratified smooth two-phase flow using the immersed interface method. Computers & Fluids, submitted for publication.

Biberg, D., 1999. Two-phase stratified pipe flow modelling—a new expression for the interfacial shear stress. In: The 2nd International Symposium on Two-Phase Flow Modelling and Experimentation, Pisa, Italy, May 22–26.

Cebeci, T., Smith, A.M.O., 1974. Analysis of Turbulent Boundary Layers. Academic Press, New York.

Charnock, H., 1955. Wind stress on a water surface. Q. J. Roy. Meteorol. Soc. 81, 639–640.

Chen, H.C., Patel, V.C., 1988. Near-wall turbulence models for complex flows including separation. AIAA J. 26, 641–648.

Chesshire, G., Henshaw, W.D., 1990. Composite overlapping meshes for the solution of partial differential equations. J. Comput. Phys. 90, 1–64.

Colebrook, C.F., 1939. Turbulent flow in pipes, with particular reference to the transition region between the smooth and rough pipe laws. J. Instn. Civil Engrs. 11, 133–156.

Demuren, A.O., Rodi, W., 1984. Calculation of turbulence-driven secondary motion in non-circular ducts. J. Fluid Mech. 140, 189–222.

Durbin, P.A., Medic, G., Seo, J.-M., Eaton, J.K., Song, S., 2001. Rough wall modification of two-layer k–ε. J. Fluid Eng. 123, 16–21.

Espedal, M., 1998. An experimental investigation of stratified two-phase pipe flow at small inclinations. Dr.Ing.-thesis, Norwegian University of Science and Technology, Department of Applied Mechanics, Thermo- and Fluid Dynamics, Trondheim, Norway.

Issa, R.I., 1988. Prediction of turbulent, stratified, two-phase flow in inclined pipes and channels. Int. J. Multiphase Flow 14, 141–154.

Ligrani, P.M., Moffat, R.J., 1986. Structure of transitional rough and fully rough turbulent boundary layers. J. Fluid Mech. 162, 69–98.

Liné, A., Masbernat, L., Soualmia, A., 1996. Interfacial interaction and secondary flows in stratified two-phase flow. Chem. Eng. Commun. 141–142, 303–329.

Lorencez, C., Nasr-Esfahany, M., Kawaji, M., Ojha, M., 1997. Liquid turbulence structure at a sheared and wavy gas–liquid interface. Int. J. Multiphase Flow 23, 205–226.

Martin, D.F., Cartwright, K., 1996. Solving Poisson's equation using adaptive mesh refinement. Technical Report UCB/ERI M96/66, U.C. Berkeley, California, USA. Available from: <http://seesar.lbl.gov/ANAG/staff/martin/AMRPoisson/>.

Meknassi, F., Benkirane, R., Liné, A., Masbernat, L., 2000. Numerical modeling of wavy stratified two-phase flow in pipes. Chem. Eng. Sci. 55, 4682–4697.

Newton, C.H., Behnia, M., 2000. Numerical calculation of turbulent stratified gas–liquid pipe flows. Int. J. Multiphase Flow 26, 327–337.

Newton, C.H., Behnia, M., 2001. A numerical model of stratified wavy gas–liquid pipe flow. Chem. Eng. Sci. 56, 6851–6861.

Nikuradse, J., 1933. Strömungsgesetze in rauhen Röhren, VDI Forschungsheft, no. 361. English translation, NACA-TM 1292, 1950.

Osher, S., Sethian, J.A., 1988. Fronts propagating with curvature-dependent speed: Algorithms based on Hamilton–Jacobi formulations. J. Comput. Phys. 79, 12–49.

Patel, V.C., Yoon, J.Y., 1995. Application of turbulence models to separated flow over rough surfaces. J. Fluid Eng. 117, 235–241.

Rosant, J.M., 1983. Ecoulements diphasiques liquide–gaz en conduite. Etude de la configuration stratifiée au voisinage de l'horizontale. Thèse de Docteur ès Sciences, Ecole Nationale Supérieure de Mécanique de Nantes, France.

Rotta, J., 1962. Turbulent boundary layers in incompressible flow. Prog. Aerosp. Sci. 2, 1–219.

Russel, T.W.F., Etchells, A.W., Jensen, R.H., Arruda, P.J., 1974. Pressure drop and holdup in stratified gas–liquid flow. AIChE J. 30, 664–669.

Shoham, O., Taitel, Y., 1984. Stratified turbulent–turbulent gas–liquid flow in horizontal and inclined pipes. AIChE J. 30, 377–385.

Strand, Ø., 1993. An experimental investigation of stratified two-phase flow in horizontal pipes. Dr.Scient. thesis, University of Oslo, Department of Mathematics, Mechanics Division, Oslo, Norway.

Taitel, Y., Dukler, A.E., 1976. A model for predicting flow regime transitions in horizontal and near horizontal gas–liquid flow. AIChE J. 22, 47–55.

Wolfshtein, M., 1969. The velocity and temperature distribution in one-dimensional flow with turbulence augmentation and pressure gradient. Int. J. Heat Mass Transfer 14, 301–318.